IET Signal Processing

*Research Article*

IET Journals
The Institution of Engineering and Technology

# Improved phase curvature autofocus for stripmap synthetic aperture radar imaging

ISSN 1751-9675
Received on 31st July 2020
Revised 17th November 2020
Accepted on 15th January 2021
doi: 10.1049/iet-spr.2020.0334
www.ietdl.org

*Jamal Saeedi*[1] ✉

[1]*Dalle Molle Institute for Artificial Intelligence (IDSIA USI-SUPSI), Lugano, Switzerland*
✉ *E-mail: jamal.saeedi@yahoo.com*

**Abstract:** Based on the theory of phase curvature autofocus (PCA) on stripmap synthetic aperture radar (SAR), an improved algorithm for increasing the accuracy of phase error compensation is presented in this study. PCA method was proposed to extend the phase gradient autofocus method for SAR systems in stripmap mode. The main problems concerned with the traditional PCA algorithm are related to selecting candidates in the image for phase error estimation, windowing, estimation procedure, and range shift due to the phase error. In this study, the modification of traditional PCA algorithm has been performed in different steps including the following: improving range-compressed data, prominent points extraction, adaptive windowing, weighted maximum likelihood for phase error estimation, improving phase error result, range shift compensation, and determining the condition to end the iterations. Real data experiments demonstrate the success of the proposed autofocus method, which is applied to the stretched-based pulsed mode SAR data set in the absence of highly accurate inertial navigation units.

## 1 Introduction

Compensation for adverse variations in the synthetic aperture radar (SAR) phase history is a major challenge in SAR signal processing development. Main reasons for these phase variations consist of oscillator and other subsystem phase instabilities, uncompensated sensor motion, and atmospheric propagation. SAR image formation of data with uncompensated phase errors causes a severe loss of geometry accuracy and degrades image quality. To avoid this, an inertial navigation unit (INU) and a global positioning system (GPS) are usually used to provide real-time data for motion compensation (MC) in SAR systems [1]. In order to achieve highly precise MC, these measurements have to be executed from pulse to pulse at sub-wavelength scale. This would surpass the accuracy of navigation systems. However, low-rate motion measurements systems provide only coarse MC, e.g. removal of partial phase error and the residual range cell migration [2, 3].

After navigation-based MC, autofocus methods are usually applied to enhance image focus by compensating residual phase error [4]. Autofocus can be described as the process of automatic estimation and compensation of residual phase error in SAR images. In general, autofocus methods can be divided into two categories: parametric and non-parametric. Parametric autofocus methods try to estimate the coefficients of an expansion that models the phase error. The mapdrift (MD) and multiple aperture mapdrift are among the best parametric autofocus techniques [5]; the performance of these algorithms is only assured when the phase error is properly modelled. These types of methods are often unable to compensate for high-frequency phase errors because of inaccurate modelling.

Non-parametric autofocus techniques do not require exact information of the phase errors for estimation. The eigenvector [6] and phase gradient autofocus (PGA) [7] algorithms are among the non-parametric methods that are able to estimate phase errors with higher order. PGA is a non-parametric method, which was first proposed in 1989 for spotlight mode SAR image formation [8]. It uses the redundancy of the phase error across many range cells by averaging them, and it is derived using maximum likelihood (ML) estimation algorithm. However, the PGA method cannot be directly applied for image formation of the conventional stripmap mode signal. Commonly, phase curvature autofocus (PCA) is applied for stripmap geometry [7, 9, 10]. Wahl *et al.* [11] proposed PCA to extend PGA for stripmap mode SAR systems.

In this study, an improved version of PCA is proposed for autofocusing of stripmap SAR mode imagery. The PCA is a well-known algorithm with great potential to deal with high-order phase error. However, there are some problems concerned with the traditional PCA algorithm, which can be mentioned asfollows: (i) the phase curvature in PCA is noisier than the phase gradient of PGA. This could be problematic for phase curvature estimation at low signal-to-clutter ratio (SCR) [12]. For this reason, selecting the strongest target on each range line is not a robust way to estimate phase error. (ii) Non-coherent averaging is used in PGA for automatic selection of the window width. However, this method cannot be applied for the PCA algorithm. Unlike PGA, the windowed targets in the PCA algorithm are not circular shifted. (iii) The model is used in the classic PCA algorithm for phase curvature estimation, supposed that the signal is made of a single point target plus clutter. However, if this assumption does not hold then the performance of the average estimator will degrade [7]. (iv) Almost all of the autofocus algorithms including PCA try to estimate the phase error and compensate for it using complex phase multiplication with range-compressed data. However, it will be theoretically shown in the paper that there is a range shift due to the phase error that should be compensated along with phase compensation. Specifically, the modification of traditional PCA algorithm has been applied in different steps consisting of the following: improving range-compressed data, prominent points (PPs) extraction, adaptive windowing, weighted ML for phase-error estimation, improving phase error result, range shift compensation, and determining the condition to end the iterations.

There are a number of similar methods that have been used to modify PGA and PCA for stripmap mode SAR autofocus. Leier *et al.* [13] argue that the PCA algorithm does not work properly in the case of wideband signals, especially for sonar applications, and proposed an improved version of PGA for stripmap SAR. The main novelty is to use overlapping sub-images to estimate phase error. The use of sub-image is partly similar to the proposed PPs extraction step here; however, they do not use PP for phase error estimation. In addition, there is no real data for evaluation of their proposed algorithm, which is another drawback. Zhang *et al.* [14] proposed a robust MC algorithm to estimate the residual phase error after coarse MC. It is partly similar to our proposed method especially in the use of sub-images and polynomial fitting over phase error. However, the method focuses on PGA instead of PCA. One drawback of using PGA for stripmap mode data is the

conversion of data into the spotlight representation. The authors argue that the PCA owing to its double differentiation characteristics is inherently less robust than PGA. Leier *et al.* in [13] mentioned that the phase curvature in PCA because of its double differentiation is sensitive to noise rather than the phase gradient of PGA. In the proposed algorithm, we aim to overcome this problem using PP selection. In addition, we have used wavelet-based denoising instead of the polynomial fitting for phase error smoothing.

Callow *et al.* [15] proposed an improved version of PGA for stripmap data autofocus. Stripmap PGA is based on estimating the local linear sway. This algorithm works on wavenumber [two-dimensional (2D) frequency] domain. De-Macedo *et al.* [12] proposed a modified version of PCA named as weighted PCA (WPCA) for autofocusing of SAR data in repeat-pass interferometry mode. The paper was a comparison between an algorithm that requires two co-registered images to reduce phase errors and an improvement of PCA that removes residual errors accurately that interferograms between images focused using the improved PCA require no additional phase correction. One similar step to the proposed method is using a weighted kernel. However, the weighted kernel for phase error estimation was originally proposed by Ye *et al.* [16] for PGA algorithm. The proposed method is formulated for autofocusing SAR data in stripmap stretched pulsed mode, however, WPCA was used for autofocusing of SAR data in repeat-pass interferometry mode. In addition, the proposed method is applied to the stretched-based pulsed mode SAR data set in the absence of highly accurate INUs, however, in WPCA, a very high-quality navigation data was being used.

SAR system can be generally be classified into two operating types including pulsed and continuous wave (CW) modes. The conventional type of SAR is the pulsed mode, which transmits short pulses. When the SAR system is continuously transmitting, the pulse length will be maximised. This requires bistatic operation in which one antenna continuously transmits and another antenna receives. These systems dechirp a return from a point scatterer using a delayed, inverse replica of the transmitted pulse [17]. This dechirped signal is sinusoidal with a frequency that depends on the distance between the point target and the sensor. Range compression is simply achieved with a Fourier transform (FT). Dechirping technique can be used in a similar manner for a pulsed mode SAR system. This method is known as stretch processing [18], which mixes received signal with a delayed, inverse replica of the transmitted signal in order to reduce the bandwidth required for sampling. Similar to CW mode SAR, range compression is achieved with an FT. In this study, the SAR image data set is in the stripmap stretched pulsed mode. As a result, the formulation and modelling in the paper have been performed for this mode. However, the proposed algorithm will work for CW or traditional pulsed mode SAR.

Our main contributions are summarised as follows:

- The problems concerned with the traditional PCA algorithm have been recognised and clearly stated in this paper including the following: (a) the noisy phase curvature, (b) the non-coherent averaging for window width selection, (c) the naïve model for phase error estimation, and (d) ignoring range shift due to the phase error.
- The modification of traditional PCA algorithm has been performed on different steps consisting of the following: improving range-compressed data, PPs extraction, adaptive windowing, weighted ML for phase error estimation, improving phase error result, range shift compensation, and determining the condition to end the iterations.
- It is shown theoretically that there is a range shift due to the phase error that should be compensated along with phase compensation.
- A new criterion based on residual motion error is proposed here to end the PCA iteration, which is theoretically shown to be optimal.
- The proposed method is formulated here for stripmap stretched pulsed mode.

The rest of this paper is structured as follows. The basic information of SAR signalling with stretch processing is briefly reviewed in Section 2. Section 3 gives the description of the proposed autofocus algorithm based on phase curvature. Section 4 illustrates experimental results in which the proposed method is tested with real data from an experimental SAR system in pulsed mode. Finally, conclusions are given in Section 5.

## 2 SAR imaging with stretch processing

As it has mentioned in Section 1, in the pulsed mode SAR with stretch processing, the similar technique to analogue dechirp (in CW mode SAR) is used to reduce the bandwidth of the received signal. In the pulsed mode radar system based on stretch processing, the LFM waveform is generated using the signal generator system with a duration more than the required system pulse width (PW). Then, the LFM signal is multiplied by a rectangular pulse to generate the pulsed signal. After being amplified by a power amplifier (PA), the signal is passed to the antenna through a circulator for transmitting ($S_t(t)$). Finally, the received or echoed signal ($S_r(t)$) after being passed through a low noise amplifier (LNA) module, is mixed with LFM signal ($S_{ref}(t)$), to obtain the stretched signal ($S_{st}(t)$).

After stretching the received signal, it can be mixed down via an appropriate intermediate frequency (IF) $f_{im}$ for digital sampling using analogue-to-digital converter (A/D). An efficient signal-processing trick that can be used to shift a signal centred at $f_{im}$ to $f_s/4$ is to specifically choose a sample rate that satisfies the following:

$$f_s = 4\ f_{im}/3 \tag{1}$$

where $f_S$ is the sampling frequency and $f_{im}$ is the centre frequency of the stretched signal.

The signal is transmitted in the form of LFM waveform, in which the signal spans the desired bandwidth over the pulse length. This is repeated at a constant rate named the pulse repetition frequency (PRF). Before transmission, the SAR signal, generated at or near baseband, should be mixed up to the desired operating frequency, $f_0$. The transmitted LFM signal can be formulated as [19]:

$$S_t(t) = A(t) \cdot \exp\left(j\left(2\pi f_0 t + \pi k_r t^2 + \varphi_0\right)\right) \tag{2}$$

where $A(t)$ is the signal amplitude as a function of time $t$, which defines the pulse length with a rect function, $f_0$ is the frequency at the beginning of the chirp, $k_r$ is the chirp rate, and $\varphi_0$ is the initial phase that can usually be neglected.

In order to generate an image with good quality, the transmitted signal needs to have enough power with large enough signal-to-noise ratio (SNR). Therefore, in the transmission chain, a PA increases the power to a predetermined level. The amplified signal transmitted through the antenna propagates to the target area. A very small portion of the transmitted signal is reflected back to the SAR antenna. The echoed signal from the target can be formulated as

$$S_r(t,\eta) = A'(t) \cdot \exp\left(j\left(2\pi f_0(t-\tau) + \pi k_r(t-\tau)^2\right)\right) \tag{3}$$

where $A'(t)$ is an attenuated version of $A(t)$, $t$ is fast time, $\eta$ is slow time or azimuth time, and $\tau$ is the two-way time of flight to the target at range $R$. Note that $\tau$ is a function of fast time $t$ and slow time $\eta$, and it is obtained as follows:

$$\tau(t,\eta) = 2R(t,\eta)/c = 2\sqrt{r_0^2 + (v(t+\eta) - y_0)^2}/c \tag{4}$$

where $v$ is the platform speed, $y_0$ is the target position in the azimuth direction, $r_0$ is the closest approach from platform to the target, and $c$ is the speed of light in the atmosphere.

The received signal is amplified with an LNA and is mixed with a copy of the transmitted signal, and finally band-pass filtered in

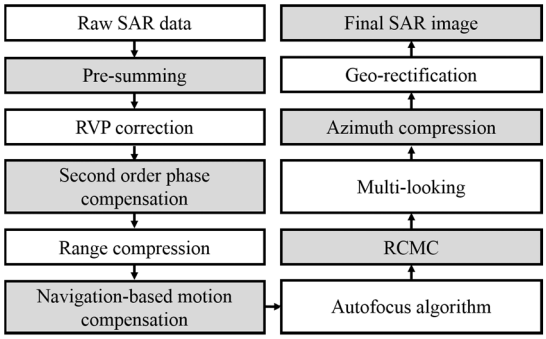


**Fig. 1** *Flow diagram of the SAR image formation algorithm*

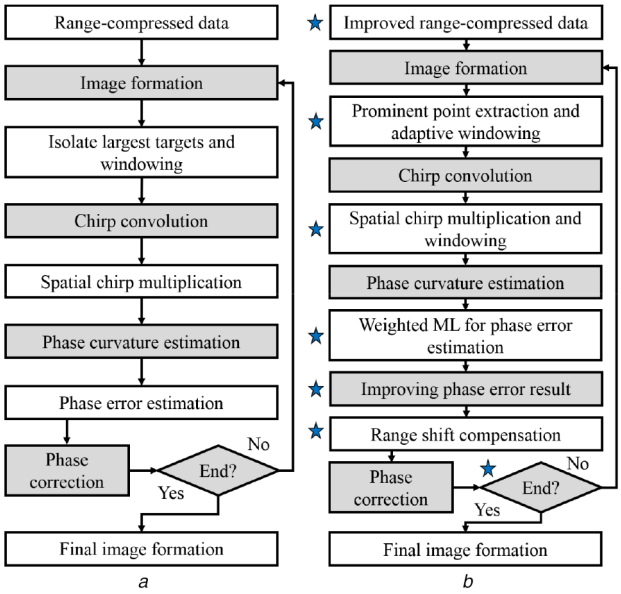


**Fig. 2** *Flow diagram of*
***(a)*** Classic PCA, ***(b)*** Improved PCA algorithms (the star markers indicate the new steps applied as compared to the classic PCA)

hardware. This is mathematically equivalent to multiplying (2) by the complex conjugate of (3). This results in the stretched signal:

$$S_{\mathrm{st}}(t,\eta) = S_{\mathrm{t}}(t)\cdot S_{\mathrm{r}}^{*}(t) = A''(\mathrm{t})\cdot \exp\left(\mathrm{j}\left(2\pi f_0\tau + 2\pi k_{\mathrm{r}} t\tau - \pi k_{\mathrm{r}}\tau^2\right)\right) \quad (5)$$

where $A''(t)$ is an amplified version of $A'(t)$, and $*$ is the complex conjugate.

Then, the stretched signal is mixed down to an appropriate frequency band for digital sampling. After the signal from (5) is mixed down by an appropriate frequency, $f_1$, the signal is ready to be digitised can be formulated as:

$$S'_{\mathrm{st}}(t,\eta) = A''(\mathrm{t})\cdot \exp\left(\mathrm{j}\left(2\pi f_0\tau - 2\pi f_1 t + 2\pi k_{\mathrm{r}} t\tau - \pi k_{\mathrm{r}}\tau^2\right)\right) \quad (6)$$

where $f_1$ is a local frequency that is used for mixing down the stretched signal to an IF, $f_{\mathrm{im}}$, for digital sampling using (1).

In order to determine the appropriate local frequency to mix down the stretched signal, the maximum and minimum frequencies related to it should be obtained:

$$f_{\max} = 2k_{\mathrm{r}}R_{\max}/c \quad (7)$$

$$f_{\min} = 2k_{r}R_{\min}/c \quad (8)$$

Then, $f_1$ is obtained using the following:

$$f_1 = f_{\max} - f_{\mathrm{im}} - [(f_{\max} - f_{\min})/2] \quad (9)$$

SAR systems can digitise this data using IF sampling as explained earlier. This data can be stored in an external hard drive on-board and be transmitted to a ground station for processing, or it can be processed on-board. Fig. 1 shows the required steps in the proposed algorithm for SAR image formation from stretched data [17]. The details about the image formation can be found in other literatures and are not discussed here anymore. The autofocus step for phase error compensation will be explained in the next section.

## 3 Proposed autofocus method

The classic PCA algorithm has a similar procedure to PGA to obtain data in aperture domain appropriate for phase error estimation. In this procedure, each point target in the image domain should be isolated, windowed, and convolved with the appropriate inverse FM chirp. This will efficiently reconstruct the range-compressed data accompanied by noise from the clutter included in the window. The reconstructed range-compressed data is then multiplied by the pre-known conjugate chirp values at each position. This results in an aperture domain data, which consists of a target-dependent complex constant multiplied by a complex exponential corresponding with the phase error. Finally, a collection of selected point targets yields a set of displaced apertures in the range-compressed domain, each of which discloses a specific portion of the phase error function.

### *3.1 Classic PCA*

The apertures are offset from each other in stripmap SAR mode in contrast with the spotlight case. These partially overlapping apertures that span different sections of the phase error function will not have the same phase gradients in the overlapping area. However, in theory, the phase curvature will approximately match for all of the apertures (related to point targets) that overlap a certain point and this is used as the basic concept for coherent averaging. This is because of the fact that phase curvature calculation can eliminate both the linear phase trend and unknown offset available in SAR signal model after chirp convolution to allow across-track averaging, while phase gradient can only omit the unknown offset from the signal. Therefore, the stripmap autofocus algorithm should compute phase curvature, averages across the apertures of prominent targets, and applies an integration to obtain an estimate of the phase error function. In the following, the critical steps of the PCA method have been described consisting of the largest targets isolation, windowing, second phase derivative estimation, and iterative correction. These steps are shown in the flow diagram of Fig. 2*a*.

*Isolate largest targets and windowing*: After initial image formation using single-look azimuth compression, the PCA algorithm attempts to isolate a number of single targets in the image for employing it in the estimation process. Here, the range Doppler algorithm (RDA) is used to generate an initial image and in each iteration for image formation. Range cell migration correction (RCMC) is a time-consuming step of RDA and it is not reasonable to apply it in each iteration of the autofocus algorithm. The range of cell migration has nothing to do with the phase error. Here, RDA is used without the RCMC step for phase error estimation in each iteration. After phase error correction from the signal in range-Doppler domain, the RCMC step has been applied and the final image has been formed, as shown in Fig. 1. A nominal procedure for selecting targets is to choose one on each across-track position. Strong targets compared to the surrounding clutter certainly considered better candidates for phase error estimation than other targets. Therefore, PCA selects the strongest target on each line.

The next step in PCA is the windowing operation, which preserves the information contained in the largest target describing the blurring kernel, while at the same time neglecting information from all other surrounding clutter and targets. The PCA algorithm simply applies a rectangular window to the data, which has the effect of rejecting data outside the window and weighting all data inside the window using a window function:

$$g(x,y) = w(y - y_{\mathrm{m}}) \cdot \tilde{f}(x,y) \tag{10}$$

where $\tilde{f}(x,y)$ is the complex SAR image, $w(y)$ is the window function, $y_{\mathrm{m}}$ is the largest target position at each across-track position $x$.

*Chirp convolution*: Unlike PGA, the windowed targets in the PCA algorithm are not circular shifted. This circular-shifting operation in PGA algorithm will preserve the effect of the phase error on the selected target while at the same time eliminating any linear phase error component (in the azimuth dimension of the range-compressed domain) associated with that target. However, there are two steps in PCA algorithm to do the same procedure as in PGA method for phase error estimation. The first step is chirp convolution, in which the windowed image, $g(x,\ y)$, is convolved with azimuth chirp suitable for each position in azimuth direction. This can be shown as:

$$\begin{aligned} c_0(x,y) = g(x,y) \odot_y \exp\left(\frac{\mathrm{j}4\pi\sqrt{r^2+y^2}}{\lambda}\right) \simeq \mathscr{F}_{f_{\mathrm{a}}}^{-1} \\ \left\{ g(x,f_{\mathrm{a}}) \cdot \exp\left(\frac{\mathrm{j}4\pi\ r\ D(f_{\mathrm{a}})}{\lambda}\right)\right\} \end{aligned} \tag{11}$$

where $r$ is closest approach from platform to the target, $r = \sqrt{x^2+h^2}$, $\odot_y$ is convolution in azimuth direction, which is equivalent to multiplication in FT domain, $f_{\mathrm{a}}$ is azimuth frequency and $\mathscr{F}_{f_{\mathrm{a}}}^{-1}$ is inverse FT. $D(f_{\mathrm{a}})$ is obtained using [17]:

$$D(f_{\mathrm{a}}) = \sqrt{1 - \left(\frac{c f_{\mathrm{a}}}{2v f_0}\right)^2} \tag{12}$$

The final stage in RDA is azimuth compression, which focuses the target in azimuth direction (Meta *et al.*[17]). The windowed and azimuth-chirped signal, $c_0(x,\ y)$, can be viewed as the result of the range-Doppler algorithm minus the final phase multiplication step [11]. In another words, the SAR image is decompressed in azimuth direction in chirp convolution step. Phase information previously hidden in blurred point targets in the image, $f(x,\ y)$, has been spread out to the width of the beam in the azimuth direction in the azimuth-chirped data $c_0(x,\ y)$.

*Spatial chirp multiplication*: Multiplying the azimuth-chirped signal with the conjugate of the spatial chirp used for the convolution is the next step in the PCA algorithm:

$$c_1(x,y) = c_0(x,y) \cdot \exp\left(-\mathrm{j}4\pi\sqrt{r^2+y^2}/\lambda\right) \tag{13}$$

which eliminates the hyperbolic phase variation of each point target using phase matching for a target at along-track position $y_{\mathrm{m}} = 0$. This step will leave a linear phase trend across each target that is dependent on its along-track position, $y_{\mathrm{m}}$ [20].

*Phase curvature estimation*: The model for the windowed and transformed data can be formulated as:

$$c_1(x,y) \simeq a(x)\mathrm{e}^{\mathrm{j}(\phi(y)+k_1 y+k_2)} + \eta(x,y) \tag{14}$$

where $x$ represents the range line, $y$ is the aperture position index, $\phi(y)$ is phase noise and $k_1$ and $k_2$ are constants. Note that the target complex reflectivity $a(x)$ is different for each range line. The noise term $\eta(x,y)$ models the interfering clutter that surrounds a selected point target. The data set is composed of $N$ range lines and $M$ cross-range columns. The noise $\eta(x,y)$ is assumed to be zero mean, white, Gaussian and independent of the signal term $a(x)$.

Equation (14) is actually an approximate relationship in order to show the signal model after spatial chirp multiplication. After this step, the phase curvature calculation is performed to eliminate both the linear phase trend and unknown offset in order to allow across-track averaging step for phase error estimation.

A straightforward method to estimate the phase error is to use all $N \times M$ data points to obtain an ML estimate of $\phi(m)$. In practice, the phase difference is estimated using only two adjacent pulses at a time. Then, it is integrated to obtain an estimate for the entire $\phi(m)$ [10]. Note that there is a linear phase trend in (14) that should be eliminated for phase error estimation. For this reason, the phase curvature of the phase in (14) should be calculated. The phase curvature is estimated in an ML sense using the following (it is proved in Appendix A by Pat in [20]):

$$\widehat{\Delta_\eta^2}(x,y) = c_1(x,y-\Delta y)\ .\ c_1^*(x,y)^2 c_1(x,y+\Delta y) \tag{15}$$

where $\Delta y$ is typically selected to be one the sample. Unlike PGA, the windowed targets in the PCA algorithm are not circular shifted. This circular-shifting operation in PGA algorithm keeps the effects of the phase error on the selected target while at the same time eliminating any linear phase error component corresponding with that target. Therefore, for PGA the phase gradient (first derivative in along-track direction) can be used to remove the unknown offset for across-track averaging and phase error estimation. However, the phase curvature calculation in PCA is necessary to eliminate both the linear phase trend and unknown offset available in SAR signal model after chirp convolution (14) to allow across-track averaging for phase error estimation.

*Phase error estimation*: Having the phase curvature estimate, it is averaged for each across-track position [20]:

$$\widehat{\Delta^2\phi}(y) = \mathrm{Arg}\left\{\int \widehat{\Delta_\eta^2}(x,y)\mathrm{d}x\right\} \tag{16}$$

This is an unbiased estimation and is efficient over a broad range of SNR [7, 20]. The phase error estimate is then obtained using double integration of the average phase curvature

$$\hat{\phi}(y) = \int \widehat{\Delta\phi}(y')\mathrm{d}y',\ \hat{\phi}(0) = 0, \tag{17}$$

where $\widehat{\Delta\phi}(y)$ is obtained using the following:

$$\widehat{\Delta\phi}(y) = \int \widehat{\Delta^2\phi}(y')\mathrm{d}y',\ \widehat{\Delta\phi}(0) = 0, \tag{18}$$

since the phase curvature was calculated using differences, the integration should be calculated as summation.

*Correcting and iterating*: In this step, the degraded range-compressed data is multiplied by the complex conjugate of our phase-error estimate

$$\bar{S}_{\mathrm{rc}}(x,y) = S_{\mathrm{rc}}(x,y)\mathrm{e}^{-\mathrm{j}\hat{\phi}(y)} \tag{19}$$

where $\bar{S}_{\mathrm{rc}}(x,y)$ denotes the corrected range compressed data.

After phase error correction, all that remains is to transform the corrected range-compressed data to the image domain by azimuth compression. Then, the algorithm iterates from step one, in which the width of the applied window $w(y)$ can be decreased at each iteration similar to the PGA method [7]. The algorithm is iterated until the estimated position error $\hat{\phi}(y)$ converges.

### *3.2 Improved PCA (IPCA)*

The processing steps of the proposed IPCA algorithm are shown in Fig. 2*b* and will be explained in the following in details.

*3.2.1 Improving range-compressed data:* The non-uniform antenna beam effect is occasionally visible in SAR imagery. This effect can be alleviated by estimating a simple model to the illumination profile and compensating the pixel brightness accordingly. Correcting the antenna illumination patterns often known as the radiometric calibration of SAR images. The first step for radiometric calibration is extracting an illumination profile from the SAR image. To obtain an illumination profile across the range, a representative pixel magnitude from each range should be selected. In this case, the median value can be selected from each column. This data are, next, smoothed by wavelet-based thresholding technique in three steps. (i) Compute the discrete wavelet transform or other kinds of multi-resolution transforms. (ii)

Zeroing high-frequency wavelet coefficients. (iii) Reconstruct the enhanced data using the inverse wavelet transformation. In practice, seven decomposition levels work well for this purpose. This data are then normalised by dividing each sample by data's maximum value. The inverse of this data is calculated by dividing each sample into one. Finally, the samples of each row of the original range-compressed data are now corrected by multiplication with this vector [21]. By correcting the non-uniform antenna beam on range-compressed data, the PPs extraction, as well as, phase error estimation can be performed more effectively.

*3.2.2 PPs extraction:* The phase of a point target can be considered hyperbolic, or approximately quadratic. The phase gradient will be approximately linear. By differentiating again, the phase curvature should be approximately constant. Therefore, strong point targets do not bias the phase curvature. For this reason, in the PCA method bias will be eliminated, so the full SNR that is available in the signal can be used for phase error estimation [22]. Furthermore, the phase curvature is considerably smaller than the phase gradient; thus, larger motion errors can be obtained without phase unwrapping. However, the phase curvature could be noisier than the phase gradient. Therefore, the precision of the phase curvature estimation can be degraded at low SCR. For this reason, selecting the strongest target on each range line is not a robust way to estimate phase error. It is discussed in sub-section 3.1 that the phase error in stripmap SAR mode should be obtained using partially overlapping sub-apertures that span different sections of the phase error function. Thus, selecting some PPs with better SCR in different sub-apertures can provide a better estimation of phase error.

For the proposed method, some local PPs have been considered for phase error estimation process. For local PPs selection, the initial SAR image will be segmented by $N$ sub-apertures and $M$ range blocks. $N$ is related to the synthetic aperture length, $L_{\text{syn}}$, and image length in the azimuth direction, $L_{\text{az}}$, as $N = 2 \times \left[L_{\text{az}}/L_{\text{syn}}\right]$. $L_{\text{syn}}$ is obtained as follows: $L_{\text{syn}} = \lambda R/2_{\text{az}}$, where $\lambda$ is the wavelength, $R$ is the slant-range to the resolution element and the subscript az is the resolution along the track. In addition, $M$ (range blocks number) can be manually set in different situations by an expert. In our case, we use five range blocks.

In each image's patch, a number of $N_{\text{t}}$ PPs are selected to represent the whole patch. First, points with maximum values in each range line are selected in the patch. After sorting the candidate points from large to small, the first $N_{\text{t}}$ number of them are chosen as local PPs in the corresponding patch. The PPs are used in phase error estimation process similar to the strongest target on each range line. It should be mentioned that the PP that has been selected in each patch should be larger than a predefined threshold; otherwise, it is omitted from the estimation process. Various types of earth terrain that have to be imaged by SAR system is responsible for determining of the dynamic range of that system. These types are consisting of the ocean, man-made target, sea-ice, natural vegetation and agriculture, mountain, forest, land and sea boundary. The typical value of $\sigma^0$ can be in the range of + 20 to −40 dB as stated in different literatures. Therefore, there is ∼60 dB dynamic range in a SAR image. Here, we consider targets with magnitude >35 dB below the maximum target in the image as PP for the rest of the algorithm. In case if there is no target available larger than this threshold in a patch, the maximum target will be selected as PP in that patch.

*3.2.3 Adaptive windowing:* The PCA algorithm simply applies a rectangular window to the data, which has the effect of rejecting data outside the window and uniformly weighting all data inside the window. It is important to capture all the target energy so that none of the defocus effect on the selected target is lost. However, if the window is too wide, an unnecessarily large amount of noise is considered for phase error estimation. Non-coherent averaging is one of the methods, used in PGA algorithm, for automatic determination of the window width. It is assumed that there is some redundancy for phase error function in the selected targets on all range lines. Non-coherent averaging is performed by summing the magnitude of SAR image data in range direction for every cross-range position:

$$s(n) = \sum_{k=1}^{N} |g(k,n)|^2 \tag{20}$$

where $g(k,n)$ is the circularly shifted complex image data, $N$ represents the total number of range lines, and $n$ symbolises the image domain cross-range position index (azimuth).

The window width can be estimated by thresholding $s(n)$ at some chosen level below its peak (typically the level selected is −10 dB [7]). However, this method cannot be applied to the PCA algorithm. Unlike PGA, the windowed targets in the PCA algorithm are not circular shifted for phase error estimation. In this study, we aim to use PPs with acceptable SCR for phase error estimation. For local PPs selection, the initial SAR image is segmented into $M$ range blocks and $N$ sub-apertures. The PPs selected in each patch of SAR image have different main lobe width and as a result, different window size should be used for them. Specifically, the PPs in each patch are centre shifted and then summed to obtain a high SCR impulse response function as averaged data. Then, the averaged data have been interpolated for better determining the window cut-off in the left and right directions. The window width can then be estimated by thresholding the magnitude of this averaged data at some predetermined level below its peak. Therefore, an adaptive window width can be obtained for each patch of the SAR image in each iteration of the PCA algorithm. Here, we have used 6 dB impulse response width (IRW) for determining the proper window width (specifically, left and right indexes from centre). This IRW is then multiplied by a predetermined factor to obtain the window width in each patch. This predetermined factor can also be gradually decreased according to the convergence speed and the estimation precision. In this study, we consider the predetermined factor of 8 and 5% decrease in each iteration.

Phase error in stripmap SAR mode should be obtained using partly overlapping sub-apertures that span different sections of the phase error function. Therefore, for a smooth transition between different sub-apertures and better derivation of phase error in these areas, windowing has been applied around each PP for phase error estimation. In other words, instead of equally weighting the image data around each PP using a rectangular window, the Taylor window is applied here for better phase curvature estimation. Another effect of applying the Taylor window (versus rectangular window) to the data is that it will low-pass filter and smoothen the estimated phase error. Taylor window is similar to the Chebyshev window. A Chebyshev window has the narrowest possible main lobe for a specified sidelobe level, but a Taylor window allows trade-offs between the main lobe width and the sidelobe level. The Taylor distribution avoids edge discontinuities, so Taylor window sidelobes decrease monotonically. Taylor window is typically used in radar applications, such as weighting SAR images and antenna design.

*3.2.4 Weighted ML for phase error estimation:* The model used in the classic PCA algorithm for phase curvature estimation in (14), supposed that the signal is made of a point target plus clutter with constant statistics with respect to the range. However, the performance of the ML estimator will degrade if this assumption is not fulfilled. In this study, an ML estimator weighting for each range bin is applied in which the weights are obtained by considering the average SCR of each range line. This is similar to the generalised correlation algorithm used for time-delay estimation [23]. In the generalised time-delay estimation method, a varying frequency weighting is applied, while in the generalised phase difference estimation algorithm a range weighting to the phase curvature is performed [24]. Before phase curvature estimation using the weighted ML, there should be a windowing procedure on the output of spatial chirp multiplication step. This is important specifically in stripmap mode data because PPs in a sub-aperture is used to estimate a segment of phase error function related to that sub-aperture, and doing so provides better phase

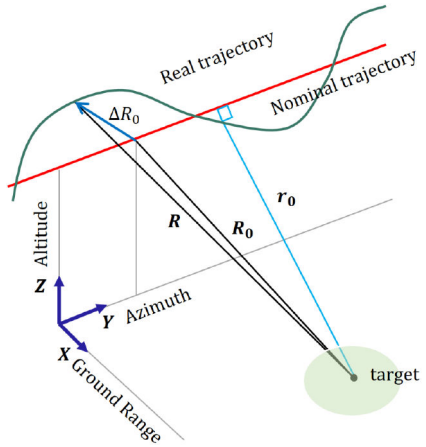


**Fig. 3** *Stripmap SAR geometry*

curvature estimation with rejecting data outside the window and weighting all the data inside

$$c_2(x_p, y) = w_p(y - y_p) \cdot c_1(x_p, y) \tag{21}$$

where $c_1(x, y)$ is defined in (14), $w_P(y)$ is the window function chosen, $x_p$ and $y_p$ are the coordinates of PPs in the image. The effective size of $w_p(y)$ can be equal to sub-aperture length chosen in the PPs extraction step.

The weighted ML estimator in contrast with the ML estimation defined in (15) for phase curvature estimation is formulated as follows:

$$\widehat{\Delta_\eta^2}(x_P, y) = \boldsymbol{W}_{ML}(x_p) \cdot c_2(x_p, y - \Delta y) \times \cdot \; c_2^*(x_p, y)^2 \cdot c_2(x_p, y + \Delta y) \tag{22}$$

where $\boldsymbol{W}_{ML}(x_p)$ is the weighting vector which is defined as:

$$\boldsymbol{W}_{ML}(x_p) = \frac{|\hat{\gamma}(x_p)|^2}{1 - |\hat{\gamma}(x_p)|^2} \cdot \frac{1}{\sum_y |c_2^*(x_p, y) \cdot c_2(x_p, y + \Delta y)|} \tag{23}$$

and

$$|\hat{\gamma}(x_p)|^2 = \frac{\sum_y |c_2^*(x_p, y) \cdot c_2(x_p, y + \Delta y)|^2}{\sum_y |c_2(x_p, y)|^2 \sum_y |c_2(x_p, y + \Delta y)|^2} \tag{24}$$

This coherence weighting formula is the same as the one that is developed for weighted phase gradient estimation proposed by Ye *et al.* [16]. Another version of the weighted ML estimator has been proposed by De-Macedo *et al.* [12] for the PCA algorithm.

*3.2.5 Improving phase error result:* The phase error function is estimated using double integration of phase curvature obtained in (22) followed by removing linear component. PCA is a non-parametric method and tries to estimate the phase error function. There is always noise in a non-parametric estimate. Noisy phase error estimations may not result in convergence of the PCA algorithm in the correcting and iterating step. It is possible to use a parametric model to fit the phase error result in order to reduce unreliable high-frequency information; however, selecting a proper model and model's parameters would be other issues. In this study, a simple wavelet-based thresholding algorithm is applied to enhance the phase error estimation results. It is similar to the method used in the antenna illumination roll-off effects estimation.

At each level of wavelet decomposition, the frequency bandwidth is divided by two. Since the initial bandwidth of the SAR signal in azimuth direction is equal to PRF, which is in our case 1000 Hz; therefore, phase noise bandwidth is up to 1000 Hz. It is obtained through the experiment that the best level to smooth the phase noise as well as keeping higher-order information is equal to five levels, which approximately cancel frequency >31.25 Hz.

*3.2.6 Range-shift compensation:* Almost all of the autofocus algorithms try to estimate the phase error and compensate it using complex phase multiplication with range-compressed data. However, it is theoretically shown that there is a range shift due to the phase error that should be compensated along with phase compensation. In order to find the range shift caused by estimated phase error, translational motion is considered in stretched signal (5). It is assumed that the translational motion causes a platform displacement from the nominal path. This results in the target scene changing in range during data collection. This means that a target at range $R_0$ measured at range $R = R_0 + \Delta R_0$ results in a phase error (shown in Fig. 3) as

$$S_{\Delta st}(t, \eta) = A''(t) \cdot \exp\big(j(2\pi f_0(\tau_0 + \Delta\tau_0) + 2\pi k_r t(\tau_0 + \Delta\tau_0) - \pi k_r(\tau_0 + \Delta\tau_0)^2)\big) \tag{25}$$

where $\tau_0 = 2R_0/c$ and $\Delta\tau_0 = 2\Delta R_0/c$.

The range-compressed signal of (25) can be a result of using FT that is formulated as follows:

$$S_{\Delta st}(t, \eta) \simeq T\text{sinc}(T(f_r - k_r(\tau_0 + \Delta\tau_0))) \times \cdot \exp(j\pi(2f_0(\tau_0 + \Delta\tau_0) - f_r(\tau_0 + \Delta\tau_0))) \tag{26}$$

Since the peak value of the range-compressed data lies on $f_r = k_r(\tau_0 + \Delta\tau_0)$, (26) can be simplified to the following formula:

$$S_{\Delta st}(t, \eta) \simeq T\text{sinc}(T(f_r - k_r(\tau_0 + \Delta\tau_0))) \times \cdot \exp\big(j\pi\big(2f_0(\tau_0 + \Delta\tau_0) - k_r(\tau_0 + \Delta\tau_0)^2\big)\big) \tag{27}$$

From (27) we can find a theoretical relation for estimated phase error as

$$\hat{\phi} \simeq -2\pi f_0\Delta\tau_0 + \pi k_r\Delta\tau_0^2 + 2\pi k_r\tau_0\Delta\tau_0 \tag{28}$$

For compensating the range shift, $\Delta\tau_0$ should be known. An estimate of $\Delta\tau_0$ can be found by solving the following second-order equation:

$$(\pi k_r)\Delta\tau_0^2 + (2\pi k_r\tau_0 - 2\pi f_0)\Delta\tau_0 - \hat{\phi} = 0 \tag{29}$$

After the phase error compensation, the range-compressed data becomes

$$\tilde{S}_{st}(f_r, \eta) \simeq T\ \text{sinc}(T(f_r - k_r(\tau_0 + \Delta\tau_0))) \times \cdot \exp\big(j\pi\big(2f_0\tau_0 - k_r\tau_0^2\big)\big) \tag{30}$$

In order to compensate the range shift due to phase error and exactly focusing the data, an azimuth-dependent interpolation should be applied here. The interpolation is defined as

$$f_r - k_r(\tau_0 + \Delta\tau_0) \rightarrow f_r' - k_r\tau_0 \tag{31}$$

To obtain perfect range compression and registration, the mapping in (31) transforms the original range frequency $f_r$ into the new range frequency, $f_r'$. By doing this, (30) can be formulated as follows:

$$\acute{S}_{st}(f_r, \eta) \simeq T\ \text{sinc}(T(f_r - k_r\tau_0)) \times \cdot \exp\big(j\pi\big(2f_0\tau_0 - k_r\tau_0^2\big)\big) \tag{32}$$

*3.2.7 Determining the condition to end the iterations:* The classic PCA algorithm is terminated when the energy of the estimated phase-error function falls below a predetermined threshold. However, this method does not consider a proper criterion to evaluate phase error correction at each iteration. In

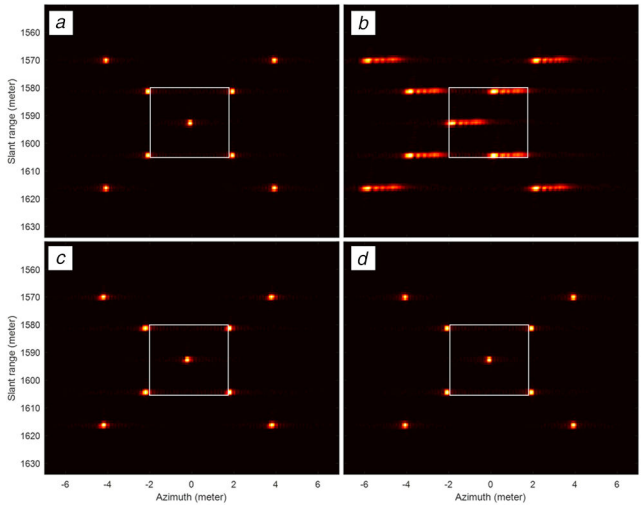


**Fig. 4** *Autofocus results for point targets simulation*
***(a)*** Amplitude image of multiple point targets obtained in ideal case, ***(b)*** Without autofocus, ***(c)*** PCA, ***(d)*** Proposed IPCA

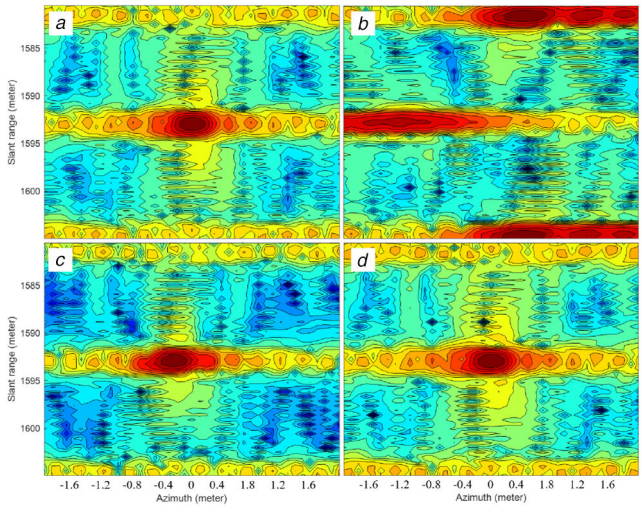


**Fig. 5** *Contour images of logarithmic scale of central target (inside white rectangles shown in Fig. 4)*
***(a)*** Ideal case, ***(b)*** Without autofocus, ***(c)*** PCA, ***(d)*** Proposed IPCA

order to avoid oscillation and to reduce the computation time, two conditions for ending the iterations are considered here. Iterations will be terminated if one of the two following conditions is fulfilled:

- Iterations will be terminated if the maximum number of iterations is reached. It should be mentioned that the iterations would not be ended if the minimum number of iterations were reached.
- After each iteration, one criterion is calculated using the translational motion due to the phase error. Iterations will be terminated if the stopping criterion reaches a value smaller than a constant threshold. Stopping criteria is defined as follows:

$$\text{Criterion: } |\Delta R(k) - \Delta R(k-1)| < T \tag{33}$$

where $k$ is the iteration number, $T$ is a threshold, and $\Delta R$ is obtained as follows:

$$\Delta R = \frac{1}{2M} c \sum_{\eta} \Delta\tau_0^2(\eta) \tag{34}$$

where $\Delta\tau_0$ is obtained using (29) and $M$ is the number of pulses.

The criterion used in the paper defined in (34) is based on residual motion error which is theoretically proved to be optimal using (29) and it is novel and never used before. The objective of autofocus is to minimise residual motion error and we aim to do the same here. Maximum and minimum iterations and the threshold for remaining motion error can be considered as parts of the setting parameters for the proposed algorithm and can be manually set in different situations by an expert.

## 4 Experimental results

This section gives results of the proposed autofocus algorithm on both simulated and real data sets acquired from an experimental SAR system. This system collects raw data with an imaging resolution of 1.5 m × 1 m (range × azimuth), which was developed by Iran in 2015. A two-seater plane carried the SAR system. The SAR system operated in X-band (9.15 GHz) with a bandwidth of 100 MHz. The plane flew at a height of ∼900–1500 m, at a speed of 30–60 m/s. At X-band, one custom microstrip antenna is used in a mono-static configuration. The antenna has an azimuth 3 dB beamwidth of 6° and an elevation 3 dB beamwidth of 35°. In this system, the returned signal is mixed with a copy of the transmitted signal to generate the stretched signal. Then, the stretched signal is mixed down via an appropriate IF, filtered and then sampled with a 12 bit A/D at 100 MHz. A custom field-programmable gate array (FPGA) board was designed to sample the signal and store the data on a pair of 32 GB compact flash disks.

In order to record all the necessary data during the flight, the data acquisition unit should start sampling at the time of return from the minimum range and stop sampling at end of return from maximum range. PRF is selected as 1000 Hz and PW is chosen as 12.5 μs. After hardware pre-summing, the effective PRF will be 333 Hz. The data window is given by time of flight far range minus time of flight near range plus pulse duration and is equal to 20 μs. Thus the data rate for a single ADC channel will be $(\text{PW} + \tau_{\max} - \tau_{\min}) \times f_s$, which is 3250 samples per echo. Consequently, the total data rate can be obtained by multiplying the data rate with the PRF and the number of bits (12 bits per sample) which is equal to 12.987 Mb/s. The SAR system was not supplied with highly accurate INU and the navigation depended only on a GPS system, which provided motion information at the frequency of 3 Hz, and positioning accuracy of 10 m. Owing to the limitation and inaccuracy of the motion information, highly precise autofocus is needed for the generation of high-quality SAR imagery.

In the first experiment, the same SAR system parameters mentioned here for the real scenario are used to generate a raw signal for multiple point targets to validate the proposed autofocus algorithm. It should be mentioned that to better demonstrate the improvement using the proposed algorithm, the simulation is performed in the noise-free condition. The results of the PCA and the proposed IPCA algorithms are shown in Figs. 4 and 5 for point target analysis. It can be observed from the results that the proposed method outperforms the PCA algorithm in terms of resolution, sidelobe levels, and accuracy of targets locations. In addition, the applied phase error to the raw signal and estimated phase errors using the PCA and the proposed IPCA have been compared in Fig. 6.

The second experiment shows the results for real SAR data set explained before. The resulted images obtained by the PCA method and the proposed autofocus approach are shown in Fig. 7, in which the vertical and horizontal directions are azimuth and range, respectively. Apparently, it can be seen from the results that the image generated by the PCA is seriously blurred and distorted in geometry. While the result obtained by the proposed autofocus method is formed with high quality. The area under observation in the image is strongly diverse partly road, agriculture, and town. The SAR image could be generated with high precision by compensating the spatially variant phases. Three local prominent targets, highlighted in Fig. 7 by the white rectangle, are amplified in the bottom left. As clearly presented in the magnified image of Fig. 7, the targets are focused in a good way for our proposed method. It can be observed that the impulse responses from point targets in azimuth direction become narrower with higher peak levels for the proposed autofocus algorithm.

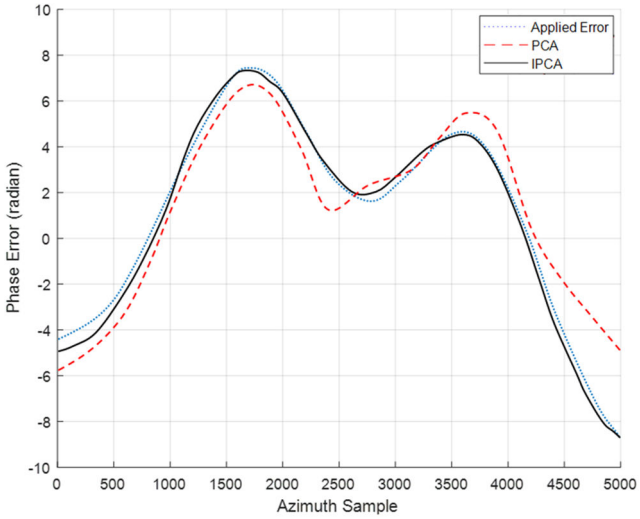


**Fig. 6** *Comparison of the PCA and IPCA phase error estimations with respect to applied phase error*

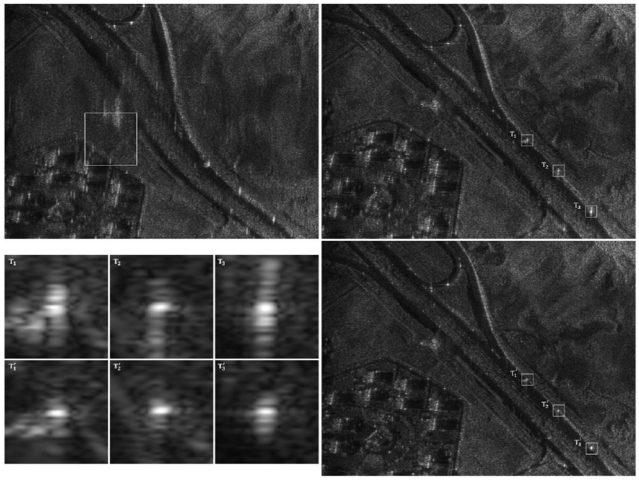

**Fig. 7** *Autofocus results, sample #1: from top left, clockwise: SAR image without autofocus, classic PCA, the proposed autofocus algorithm, and magnified target images inside the small white rectangles*

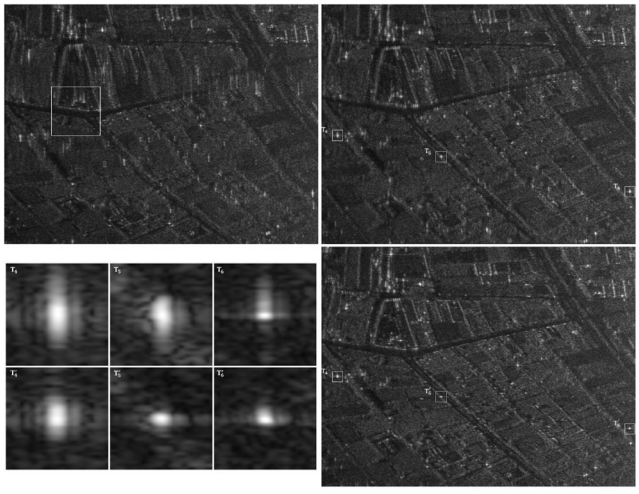

**Fig. 8** *Autofocus results, sample #2: from top left, clockwise: SAR image without autofocus, classic PCA, the proposed autofocus algorithm, and magnified target images inside the small white rectangles*

The proposed method works very well in areas with a high number of PPs. An example of a focused SAR image, created by the proposed autofocus algorithm, is shown in Fig. 8. From Fig. 8, one can see that the freeway, villages, and wild scenes clearly distinguished and well-focused. The proposed method was also

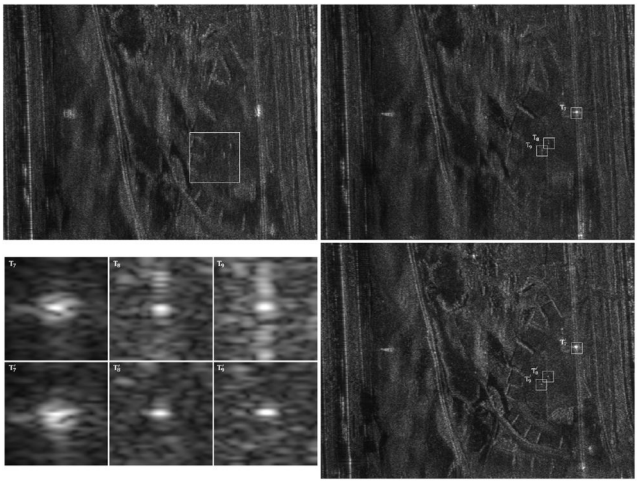

**Fig. 9** *Autofocus results, sample #3: from top left, clockwise: SAR image without autofocus, classic PCA, the proposed autofocus algorithm, and magnified target images inside the small white rectangles*

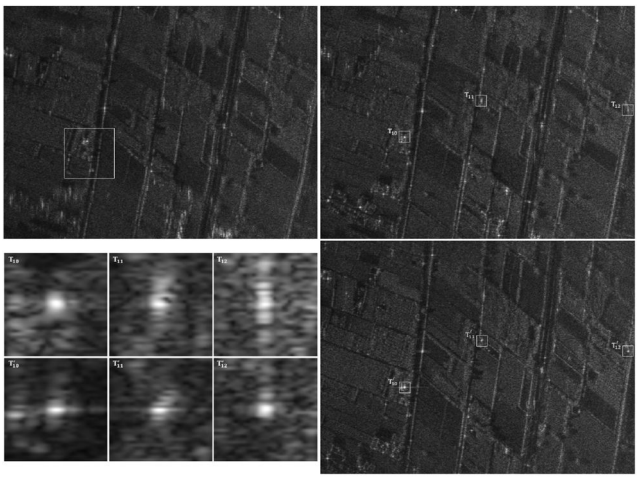

**Fig. 10** *Autofocus results, sample #4: from top left, clockwise: SAR image without autofocus, classic PCA, the proposed autofocus algorithm, and magnified target images inside the small white rectangles*

verified at homogeneous areas with a smaller number of PPs (see Figs. 9 and 10).

Table 1 shows the quantitative results associated with the point targets selected in Figs. 7–10. Three different measures including peak sidelobe level ratio (PSLR), integrated sidelobe level ratio (ISLR), and IRW are used to evaluate the performance of different autofocus algorithms. It can be clearly seen from the results that the proposed autofocus algorithm outperforms the PCA method in terms of different metrics. The average results for twelve targets based on PSLR, ISLR, and IRW metrics are as follows (left: PCA and right: IPCA): $(-5.87, -9.09)$, (7.94, 3.45), and (4.27, 3.02). Specifically, the percentages of improvement for PSLR, ISLR, and IRW for the proposed method as compared to the PCA algorithm are 54, 56, and 29%, respectively.

The residual motion error ($\Delta R$ in (34)) obtained from the phase error of PCA and IPCA methods with different data set is shown in Fig. 11. It can be seen from the result that the proposed IPCA outperforms PCA in terms of residual motion error. The residual phase error for IM #1 is not very well compensated at the beginning of azimuth time as compared with other cases. This is because of the scarcity of PPs for phase error estimation in this area of the image. In other cases, the residual motion error is insignificant.

In the third experiment, previous widely used autofocus algorithms have also been implemented and the results are compared with the proposed IPCA algorithm. Since PCA [11] and the proposed IPCA are considered as non-parametric approaches, two parametric methods are selected here for comparison: MD

**Table 1** Results of autofocus experiment for different point targets selected from Figs. 7–10. Each sample in azimuth direction is equal to 0.22 m

| Metric | Method | $T_1$ | $T_2$ | $T_3$ | $T_4$ | $T_5$ | $T_6$ | $T_7$ | $T_8$ | $T_9$ | $T_{10}$ | $T_{11}$ | $T_{12}$ |
|---|---|---|---|---|---|---|---|---|---|---|---|---|---|
| $PSLR_{dB}$ | PCA | −3.013 | −8.530 | −4.046 | −9.013 | *−12.87* | −6.750 | −4.625 | −3.328 | −3.851 | −9.729 | −3.182 | −1.588 |
| | IPCA | *−6.416* | *−9.546* | *−4.552* | *−12.64* | −12.02 | *−12.49* | *−5.889* | *−8.525* | *−8.931* | *−10.19* | *−9.821* | *−8.14* |
| $ISLR_{dB}$ | PCA | 8.823 | 6.180 | 9.978 | 4.353 | 5.170 | 5.939 | 5.017 | 10.06 | 11.12 | 3.507 | 9.759 | 15.47 |
| | IPCA | *5.149* | *0.987* | *4.458* | *3.666* | *1.692* | *0.898* | *4.268* | *5.035* | *5.542* | *−0.066* | *3.501* | *6.337* |
| $IRW_{sample}$ | PCA | 4.510 | 2.500 | 3.930 | 10.88 | 9.05 | 2.560 | *2.310* | 3.480 | 3.740 | 4.220 | 2.920 | 6.560 |
| | IPCA | *2.130* | *2.450* | *2.200* | *7.560* | *3.420* | *3.230* | 3.130 | *2.110* | *2.320* | *2.120* | *1.940* | *3.730* |

The italicised values are representing the best results for each image with respect to each metric.

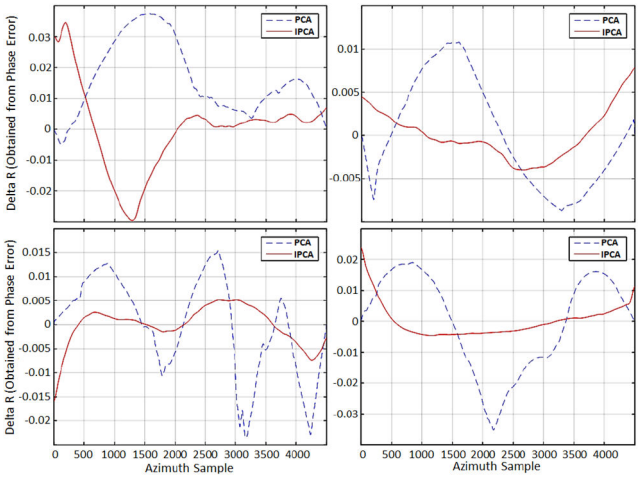


**Fig. 11** *Residual motion error (ΔR) obtained from phase error of PCA and IPCA methods with different images, left to right, top row: IM #1, IM #2; bottom row: IM #3, and IM #4*

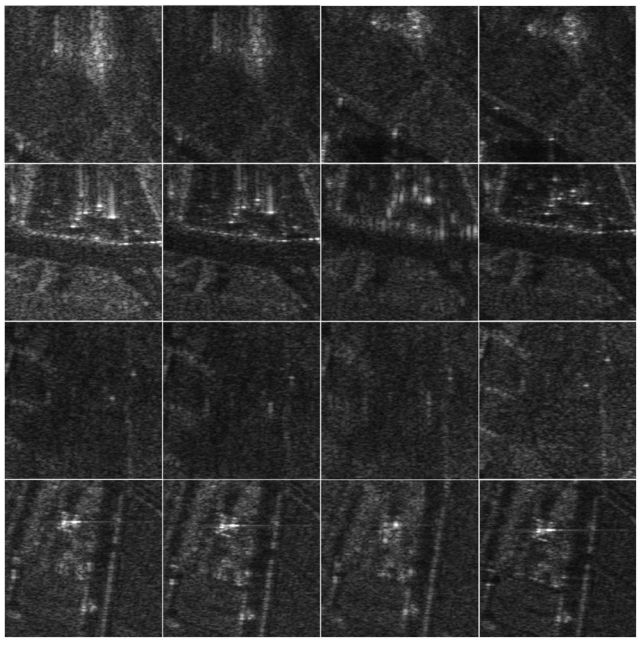

**Fig. 12** *Autofocus results, from top to bottom: magnified images selected from images #1 to #4, and from left to right: the results from the CO, MD, classic PCA, and the proposed IPCA algorithms*

algorithm [25, 26] and contrast optimisation (CO) method (which is an image metric-based autofocus algorithm) [26, 27]. Parametric autofocus methods try to estimate the coefficients of an expansion that models the phase error. In the classical CO algorithm [27], an optimisation strategy is designed through maximising contrast of the obtained image to estimate phase error parameters. The MD is based on multi-look processing and takes advantage of the fact that, in the case of mismatch between the assumed phase error model and true parameters, sub-images are out of focus and cross-range shifted. The computed cross-range shift between sub-images is used to estimate true parameters.

The four SAR images used in the second experiment have been also used for generating the results for CO and MD methods. For better clarity, the magnified images inside the large white rectangles inside top-left images of Figs. 7–10 are selected here for comparison. The resulted images obtained by different methods are shown in Fig. 12 in which the vertical and horizontal directions are azimuth and range, respectively. It can be clearly seen from the results that the images generated by the CO, MD and PCA are in most cases blurred and distorted in geometry. While the results obtained by the proposed IPCA method are formed with high quality in terms of focus and SNR. The performance of CO and MA algorithms is only assured when the phase error is properly modelled. These types of methods are often unable to compensate high-frequency phase errors because of inaccurate modelling. In addition, CO and MD need high computational power due to image creation at each iteration [28].

In the final experiment, two metrics are used to evaluate the results based on image quality. A class of autofocus algorithms optimises image sharpness metrics to improve image quality [29]. In these metric-based autofocus techniques, the phase error estimate is obtained using an optimisation method to maximise a particular sharpness metric, which is evaluated on the defocused image intensity. For this reason, sharpness index is chosen as the first metric. Blanchet and Moisan [30] proposed the image sharpness metric based on the Fourier phase spectrum, which comprises essential information about the image geometry and its contours. It is mentioned by Blanchet and Moisan [30] that measuring the amount of phase coherence in an image is associated with measuring the quality of the transitions between flat regions, that is the edges. In other words, phase coherence provides information about boundary alignment, which is related to image sharpness. The second metric is the entropy index, which measures the focus quality after phase error correction. It is well-known that the smaller the entropy value, the better the quality in focus after the phase error correction [31]. The entropy index is defined as follows [32]:

$$H = -\frac{1}{E_z}\sum_{m,n}|z_{mn}|^2\ln|z_{mn}|^2 + \ln(E_z) \tag{35}$$

where $z_{mn}$ is corresponding phase-corrected complex-valued SAR image, $E_z = \sum_{m,n}|z_{mn}|^2$, and $0 \le n < N$ and $0 \le k < N$. $m$ and $n$, are indexes in range and azimuth directions. $N$ is the total number of samples in the azimuth direction, and $M$ is the total number of samples in range direction.

Table 2 shows the quantitative results based on the two metrics consisting of entropy [32] and sharpness [30], for different images used in the second experiment. Based on the results, it can be seen that the proposed method outperforms other methods in three out of four cases for sharpness and entropy indexes.

PCA has the equivalent computational complexity of $\sim O(N \wedge 2\ \log N)$ [11]. The proposed method preforms different modifications to the classic PCA. Some of these modifications reduce the computational complexity and some will increase it. On the one hand, the number of points extracted for phase error estimation in the proposed method are smaller than the traditional PCA, which considers one target for each range line; this reduces

**Table 2** Quantitative results of autofocus methods for different SAR images

| Metric | Method | IM #1 | IM #2 | IM #3 | IM #4 |
|---|---|---|---|---|---|
| entropy | No AF | 20.257 | *20.3675* | 20.319 | 20.158 |
| | CO | 20.301 | 20.3724 | 20.307 | 20.144 |
| | MD | 20.223 | 20.3815 | 20.329 | 20.153 |
| | PCA | 20.218 | 20.3736 | 20.312 | 20.182 |
| | IPCA | *20.201* | 20.3837 | *20.300* | *20.136* |
| sharpness | No AF | 433.62 | 194.89 | 293.66 | 476.41 |
| | CO | 487.44 | 195.65 | 340.12 | *561.10* |
| | MD | 473.50 | 193.31 | 335.91 | 558.25 |
| | PCA | 517.88 | 190.87 | 323.01 | 437.07 |
| | IPCA | *582.57* | *199.30* | *354.32* | 557.91 |

The italicised values are representing the best results for each image with respect to each metric.

the computational complexity for phase error estimation. On the other hand, there are two steps in the proposed method that increases the computational complexity including: improving phase error result, and range shift compensation. Improving phase error result is a 1D wavelet-based denoising that has equivalent computational complexity of $\sim O(N \log N)$ and range shift compensation step is a 2D matrix multiplication that has the equivalent computational complexity of $\sim O(N \wedge 2)$. Therefore, it can be generally said that the proposed IPCA is computationally competitive with PCA.

## 5 Conclusions and future works

This paper presents an autofocus algorithm compatible with the pulsed mode SAR system with stretch processing in stripmap mode imaging. The proposed autofocus, which is an improved PCA algorithm, is proposed to increase the accuracy of phase error compensation. Specifically, the modification of traditional PCA algorithm has been performed on different steps including the following: improving range-compressed data, PPs extraction, adaptive windowing, weighted ML for phase error estimation, improving phase error result, range shift compensation, and determining the condition to end the iterations. Results of real data experiments demonstrate that the improved PCA algorithm outperforms the traditional one in terms of SAR image quality metrics.

For future work, we will investigate the extension of the proposed method for applying to the PGA algorithm in spotlight imaging mode as well as the SAR data acquired from CW or traditional pulsed modes.

## 6 Acknowledgment

The author thanks the anonymous reviewers for their helpful and constructive comments that significantly contributed to improving this paper.

## 7 References

[1] Saeedi, J.: 'Feasibility study and conceptual design of missile-borne synthetic aperture radar', *IEEE Trans. Syst., Man, Cybern.: Syst.*, 2020, **50**, (3), pp. 1122–1133

[2] Fornaro, G.: 'Trajectory deviations in airborne SAR: analysis and compensation', *IEEE Trans. Aerosp. Electron. Syst.*, 1999, **35**, (3), pp. 997–1009

[3] Saeedi, J., Alavi, S.M.: 'Improved navigation-based motion compensation for LFMCW synthetic aperture radar imaging', *Signal, Image, Video Process.*, 2016, **10**, (2), pp. 405–412

[4] Saeedi, J., Faez, K.: 'A back-projection autofocus algorithm based on flight trajectory optimization for synthetic aperture radar imaging', *Multidimens. Syst. Signal Process.*, 2016, **27**, (2), pp. 411–431

[5] Samczynski, P., Kulpa, K.S: 'Coherent MapDrift technique', *IEEE Trans. Geosci. Remote Sens.*, 2010, **48**, (3), pp. 1505–1517

[6] Jakowatz, C.V., Wahl, D.E.: 'Eigenvector method for maximum-likelihood estimation of phase errors in synthetic aperture radar imagery', *Opt. Lett.*, 1993, **10**, (12), pp. 2539–2546

[7] Wahl, D.E., Eichel, P.H., Ghiglia, D.C., *et al.*: 'Phase gradient autofocus — A robust tool for high resolution SAR phase correction', *IEEE Trans. Aerosp. Electron. Syst.*, 1994, **30**, (3), pp. 827–835

[8] Eichel, P.H., Ghiglia, D.C., Jakowatz, C.V.: 'Speckle processing method for synthetic aperture radar phase correction', *Opt. Lett.*, 1989, **14**, (1), pp. 1–3

[9] Eichel, P.H., Jakowatz, C.V.: 'Phase-gradient algorithm as an optimal estimator of the phase derivative', *Opt. Lett.*, 1989, **14**, (20), pp. 1101–1103

[10] Jakowatz, C.V., Wahl, D.E., Eichel, P.H., *et al.*: '*Spotlight-mode synthetic aperture radar: A signal processing approach*' (Kluwer Academic Publishers, Boston, 1996)

[11] Wahl, D., Jakowatz, C.V., Thompson, P.A.: 'New approach to stripmap SAR autofocus'. Sixth IEEE Digital Signal Processing Workshop, Yosemite National Park, CA, USA, 1994, pp. 53–56

[12] De Macedo, K.A.C., Scheiber, R., Moreira, A.: 'An autofocus approach for residual motion errors with application to airborne repeat-pass SAR interferometry', *IEEE Trans. Geosci. Remote Sens.*, 2008, **46**, (10), pp. 3151–3162

[13] Leier, S., Kronig, M., Zoubir, A.M.: 'A modified version of the mosaic phase gradient autofocus'. 21st European Signal Processing Conf. (EUSIPCO 2013), Marrakech, 2013, pp. 1–5

[14] Zhang, L., Qiao, Z., Xing, M.D., *et al.*: 'A robust motion compensation approach for UAV SAR imagery', *IEEE Trans. Geosci. Remote Sens.*, 2012, **50**, (8), pp. 3202–3218

[15] Callow, H.J., Hayes, M.P., Gough, P.T.: 'Stripmap phase gradient autofocus'. Celebrating the Past ... Teaming Toward the Future (IEEE Cat. No.03CH37492), San Diego, CA, USA, 2003, Vol. 5, pp. 2414–2421

[16] Ye, W., Yeo, T.S., Bao, Z.H.: 'Weighted least-squares estimation of phase errors for SAR/ISAR autofocus', *IEEE Trans. Geosci. Remote Sens.*, 1999, **37**, (5), pp. 2487–2494

[17] Meta, A., Hoogeboom, P., Ligthart, L.P.: 'Signal processing for FMCW SAR', *IEEE Trans. Geosci. Remote Sens.*, 2007, **45**, (11), pp. 3519–3532

[18] Schikorr, M.: 'High range resolution with digital stretch processing'. IEEE Radar Conf., Rome, 2008, pp. 1–6

[19] Saeedi, J., Faez, K.: 'Synthetic aperture radar imaging using nonlinear frequency modulation signal', *IEEE Trans. Aerosp. Electron. Syst.*, 2016, **52**, (1), pp. 99–110

[20] Pat, J.B.: 'Synthetic aperture sonar image reconstruction using a multiple-receiver towfish'. M.Sc. Thesis, Department of Electrical and Electronic Engineering, University of Canterbury, Christchurch, New Zealand, 2000

[21] Doerry, A.W.: 'Automatic compensation of antenna beam roll-off in SAR images', *SANDIA REPORT*, 2006, pp. 1–19, http://www.sandia.gov/radar/complex_data/sand20062632_antenna_beam_comp.pdf

[22] Fortune, S.A.: 'Phase Error Estimation for Synthetic Aperture Imagery', Ph.D. Dissertation, Electrical and Electronic Engineering Department, University of Canterbury, Christchurch, New Zealand, 2005

[23] Knapp, C.H., Carter, G.C.: 'The generalised correlation method for estimation of time delay', *IEEE Trans. Acoust. Speech Signal Process.*, 1976, **24**, (4), pp. 320–327

[24] Wang, Y., Zhu, X.: 'Robust estimators for multipass SAR interferometry', *IEEE Trans. Geosci. Remote Sens.*, 2016, **54**, (2), pp. 968–980

[25] Oliver, C., Quegan, S.: '*Understanding synthetic aperture radar images*' (Artech House, Norwood, MA, 1999)

[26] Kirscht, M.: 'Detection, velocity estimation and imaging of moving targets with single channel SAR'. Proc. EUSAR, Friedrichshafen Germany, 1998

[27] Berizzi, F., Dalle Messe, E., Mortorella, M.: 'Performance analysis of a contrast-based ISAR autofocusing algorithm'. Proc. IEEE Radar Conf., Long Beach CA, April 2002, pp. 200–205

[28] Samczyński, P., Pietrzyk, G., Gorzelanczyk, A.: 'Performance analysis of non-coherent methods of autofocusing images in strip mode SAR'. Proc. SPIE Photon. Appl. Astronomy, Commun. Ind. High-Energy Phys. Exp. IV, Bellingham, WA, 2006, (6159), pp. 61591M-1–61591M-7

[29] Morrison, R.L., Do, M.N., Munson, D.C.: 'SAR image autofocus by sharpness optimization: A theoretical study', *IEEE Trans. Image Process.*, 2007, **16**, (9), pp. 2309–2321

[30] Blanchet, G., Moisan, L.: 'An explicit sharpness Index related to global phase coherence'. In Proc. of the IEEE Int. Conf. on Acoustics, Speech, and Signal Processing, Kyoto, Japan, 2012, pp. 1065–1068

[31] Kragh, T.J.: 'Monotonic iterative algorithm for minimum-entropy autofocus'. Proc. 14th Annu. ASAP Workshop, Lexington, MA, USA, 2006, pp. 1–38

[32] Erdogan, H., Fessler, J.A.: 'Monotonic algorithms for transmission tomography', *IEEE Trans. Med. Imag.*, 1999, **18**, (9), pp. 801–814